Advances in carboxylate collectors adsorption on monazite surface: Part 1-Assessment of the hydroxylation and carbonation of surface lanthanide ions

Anthony Geneyton, L. O. Filippov, A. Renard, M. Mallet, Nour-Eddine Menad

Version of Record: https://www.sciencedirect.com/science/article/pii/S0169433219310098
Manuscript_55c428b5827df47e3831b624e44d70f6

Advances in carboxylate collectors adsorption on monazite surface: Part 1 – Assessment of the hydroxylation and carbonation of surface lanthanide ions

A. Geneyton [a,b], L.O. Filippov [a,*], A. Renard [c], M. Mallet [c], N.-E Menad [b]

[a] Université de Lorraine, CNRS, GeoRessources, F- 54000 Nancy, France

[b] BRGM, Water, Environment and Ecotechnologies Division, Waste and Raw Materials & Recycling Unit, 3 Avenue Claude Guillemin, BP 36009, 45060 Orléans Cedex, France

[c] Université de Lorraine, CNRS, LCPME, F- 54000 Nancy, France

*Corresponding author: lev.filippov@univ-lorraine.fr, +33 3 72 74 45 46, 2 rue du Doyen Marcel Roubault, 54500, Vandoeuvre Les Nancy

GRAPHICAL ABSTRACT

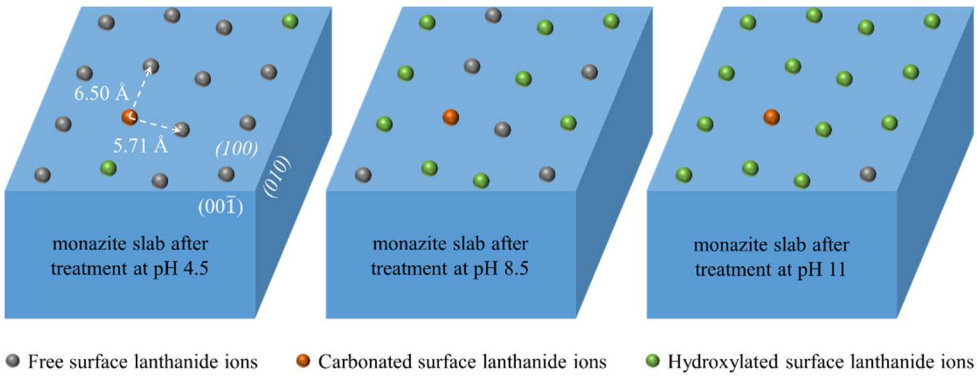

Note: Black and white should be used for any figures in print

ABSTRACT

The adsorption of carboxylate collectors is largely assumed to be affected by the monazite surface speciation. In order to provide key information for the understanding of this phenomenon, we propose in this study a thermodynamic model for the equilibrium of monazite-(La) crystal in an H_2O-CO_2 system. This model allows access to the speciation information of the dissolved lattice species. Based on this model, we identify potential chemical reactions that may affect, under certain conditions, lanthanide ions on monazite surface. Since these surface ions have vacant coordination sites, they may react with water molecules and media species to restore their coordination shells. Therefore, it has been suggested that surface lanthanide ions undergo hydroxylation and carbonation reactions under alkaline conditions.

X-ray photoelectron spectroscopy and Fourier-transform infrared spectroscopy were used to analyse synthetic monazite-(La) samples treated in deionised water or diluted sodium carbonate solutions. The spectroscopy results suggest that the surface lanthanide ions do tend to hydroxylate under alkaline conditions. Furthermore, under the tested conditions, no significant monazite surface carbonation was observed. These results indicate that surface lanthanide ions have limited affinity for dissolved carbonate species, contrary to what is suggested by the thermodynamic model for free lanthanide ions in the bulk.

KEYWORDS: Rare-earth minerals, Lanthanides, Monazite, Surface speciation, Thermodynamic, Hydroxylation

Abbreviations: DRIFT: diffuse reflectance infrared Fourier transform, FTIR spectroscopy: Fourier transformed infrared spectroscopy, XPS: X-ray photoelectron spectroscopy, XRD: X-Ray diffraction, Ln: lanthanides

1. Introduction

Carboxylates and hydroxamates are two common surfactants used as collectors in the flotation separation of rare-earth semi-soluble salts (i.e. monazite, bastnaesite, and xenotime) from their gangue minerals [1–3]. From a general perspective, the selective flotation of rare-earth semi-soluble salts from their gangue minerals using these anionic collectors is a complex issue. Therefore, extensive studies have been performed to understand their adsorption mechanisms. These collectors are reported to provide optimal performance under slightly alkaline

conditions, for which free lanthanide ions are expected to become hydroxylated in the bulk. Therefore, it has been hypothesised that hydroxylated lanthanide species are likely to enhance flotation performance when carboxylate and hydroxamate collectors are used [4–10], but their promotion mechanism is not fully understood. A commonly referenced surface activation mechanism proposed by Pradip and Fuerstenau [4] suggests that dissolved lattice lanthanide metal ions are hydrolysed to form $Ln(OH)^{2+}$ and $Ln(OH)_2^{+}$ species that re-adsorb on monazite surface. Those adsorbed species form hydroxylated surface sites that promote the adsorption of anionic hydroxamate and carboxylate collectors. Although the positive influence of hydroxylated lanthanide surface species on flotation performance is widely accepted, the mechanism of surface hydroxylation may be contested because of the naturally reduced solubility of certain rare-earth semi-soluble salts. It is more likely that surface lanthanide ions directly hydroxylate at an appropriate pH.

All assumptions regarding the active role of hydroxylated lanthanide species on the adsorption of carboxylate and hydroxamate collectors are based on the similarities between the measured pH conditions for optimal flotation performance and calculated pH conditions for the first hydroxylation of lanthanide ions in the bulk. Therefore, the proposed mechanisms of collector adsorption are based on the analysis of speciation diagrams, which reveal the predominant lanthanide species in the bulk as a function of pH. Thermodynamic models for lanthanide species predominance in the bulk are frequently suggested as relevant tools for identifying potential reactions that may affect surface lanthanide ions that have vacant coordination sites. Indeed, in the case of carbonate minerals, it has been shown that such ions are subjected to similar reaction mechanisms when they are coordinated with other lattice ions on mineral surfaces and when they are dissociated in the bulk [11,12]. Van Cappellen et al. [11] also established that the stability constants of these reactions are similar in both environments. However, there are three main limitations to the assessment of mineral surface speciation using thermodynamic models of bulk species predominance:

- The use of models including a reduced number of lanthanide species may lead to the omission of a predominant species. For example, lanthanide ions are known to have a greater affinity for carbonate groups than hydroxyl groups [13], but lanthanide carbonate species are not implemented in typical

speciation models.

- Reaction kinetics are not considered in these models, which may induce significant biases. This is especially true for sparingly soluble minerals, such as monazite.
- The ions present on mineral surfaces are coordinated with other lattice ions. Although they may present vacant coordination sites, resulting in an electron surplus or deficit, the electric charges of these surface ions are reduced, which limits the extent of certain reaction mechanisms, such as the number of hydroxides ligands bound to a surface cation compared to the expected number when the same cation is free in the bulk.

We present a series of two papers that explore further details regarding the adsorption of carboxylate collectors on monazite surface and the influence of the speciation of lanthanide surface sites. The first part of this series is focused on the assessment of the hydroxylation and carbonation of surface lanthanide ions. The second part will cover the adsorption of carboxylate collectors on monazite surface and the role of mineral surface speciation in this adsorption. In this study, beyond the conventional Pourbaix and standard speciation diagrams, a model of monazite-(La) crystal in thermodynamic equilibrium with an H_2O-CO_2 system was implemented. After identifying the number of vacant coordination sites for the lanthanide ions exposed on the monazite cleavage plane, assumptions are made regarding the potential reactions that will affect those surface ions. The presence of newly formed surface lanthanide species, such as lanthanide hydroxides and carbonates, was evaluated via XPS and FTIR spectroscopy.

2. Materials and methods

2.1. Synthetic monazite materials

XPS and FTIR analyses were performed on synthetic lanthanum monazite materials produced using lanthanum hydrated phosphate with a lanthanum content of 51.88 wt% supplied by Alfa Aesar and identified as rhabdophane analogue via XRD. The lanthanum phosphate powder was placed in a recrystallised alumina crucible and thermally treated in an electric muffle furnace following the procedure detailed in Geneyton et al. (2019) [14]. The XRD diffractogram presented in Fig. 1 confirmed a total conversion of the initial product into dehydrated lanthanum orthophosphate with the monazite structure. This diffractogram was obtained at the LIEC laboratory

(Nancy, France) using a Bruker D8-Advance diffractometer equipped with a cobalt anticathode (35 kV - 45 mA) as an X-ray emitting source (λ=1.78897 Å), θ–2θ goniometer, and LynxEye energy-dispersive one-dimensional detector. XRD analysis was performed with a 2θ angle ranging from 3–64°, step size of 0.034°, and acquisition time of 3 s.

The monazite powder was then compacted into cylindrical pellets using a cylindrical press (compaction time: 1 min, compaction pressure: 1 tonne). The pellets were then sintered at 1450 °C for 5 h and manually crushed with an agate mortar. After wet sieving with deionised water, −80+36 µm and −36 µm fractions were collected and oven-dried at 40 °C. The −80+36 µm fraction was used for experiments involving FTIR analyses, whereas the −36 µm fraction was further reduced in an agate planetary ball mill (Fritsch Pulverisette) for 2 h and used for experiments involving XPS analyses.

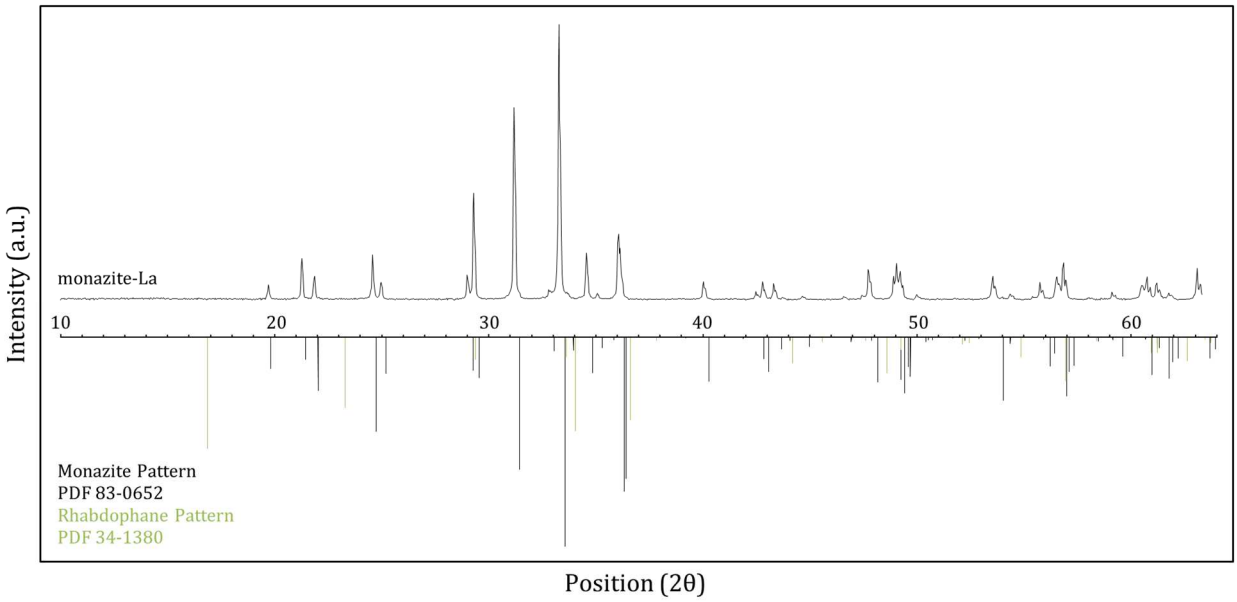

Figure 1: XRD diffractograms of the lanthanum monazite material obtained via thermal treatment of synthesised rhabdophane material

2.2. XPS

The XPS spectra of the monazite samples were acquired at the LCPME laboratory (Villers-les-Nancy, France) using a Kratos Axis Ultra DLD (Kratos Analytical, U.K.) X-ray photoelectron spectrometer equipped with a monochromatic Al Kα X-ray source (1486.6 eV) operating at 120 W. The spectra were collected at a normal take-off angle (90°) and the analysis area was 700 × 300 µm^2. The pressure in the analytical chamber was 10^{-7} Pa.

Survey scans were taken with an analyser pass energy of 160 eV in 1 eV steps and high-resolution scans were taken at a pass energy of 20 eV in 0.1 eV steps, except for the carbon and oxygen scans, which used steps of 0.05 eV. Charge correction was carried out using the adventitious carbon peak C 1s at 284.6 eV. The calculations of the XPS elemental compositions based on the main peak areas measured from the high-resolution spectra were performed using the Kratos Vision 2.2.11 software package.

Sample preparation involved the treatment of 100 mg of intensely pulverised monazite powder in test tubes (closed atmosphere) or beakers (open atmosphere) containing 35 mL of deionised water. Although the pH of the solution is, in both cases, adjusted before monazite addition, it is only maintained constant during treatment when performed in a beaker. The monazite suspensions were mixed for 1 h. The particles were then collected via filtration through a nylon filter (0.8 µm pore size) and rinsed for a few seconds with deionised water, except the particles treated with sodium carbonate solution which was rinsed for 30 seconds to limit monazite surface contamination. The powders were then placed in a desiccator for drying prior to their introduction into the spectrometer.

2.3. FTIR spectroscopy

Vibrational spectroscopy was performed at the GeoRessources laboratory using the DRIFT technique. The infrared spectra were acquired (Nancy, France) using a BRUKER EQUINOX IFS 55 spectrometer equipped with broadband (5500–600 cm^{-1}) mercury cadmium telluride detector cooled at 77 K and diffuse reflectance attachment (Harrick Corporation). Each sample was scanned for approximately 90 s with a 2 cm^{-1} spectral resolution. The influences of atmospheric water and carbon dioxide were subtracted from the final spectra. Sample preparation involved mixing 50 mg of monazite with 280 mg of spectroscopic grade potassium bromide powder. This mixture was placed in a cup inside the spectrometer.

Treatment involved mixing 200 mg of monazite-(La) powder in 40 mL of pH-adjusted deionised water for 1 h. The pH was continuously adjusted using USP-grade hydrochloric acid and sodium hydroxide. Following this treatment, the particles were collected via filtration through a nylon filter (0.8 µm pore size), rinsed with deionised water for a few seconds, then placed in a desiccator for drying.

3. Thermodynamic equilibrium calculations

3.1. Conventional models of the speciation of lanthanide in an aqueous solution

When determining the speciation of an element in an aqueous solution, Pourbaix diagrams or speciation diagrams are typically calculated. In this study, both types of diagrams were calculated for lanthanum. Given that the information expressed by these two types of diagrams are very similar, only the speciation diagram of lanthanum will be discussed in detail. To visualise the influence of the electrode potential of the solution on lanthanum speciation, the Pourbaix diagram of lanthanum may be consulted in the supporting material file (Fig. S1).

Conventionally, speciation calculations in aqueous media only consider hydroxylation reactions. In this study, a similar approach was first adopted. The speciation diagram presented in Fig. 2 was constructed with the reaction constants listed in Table 1. These constants, which were determined experimentally, are significantly affected by operating conditions. In absence of standard thermodynamic constants (i.e. extrapolated to infinite dilution), it seems more reliable to perform thermodynamic calculations using apparent constants derived from the same source. Therefore, in our study, the constants for the reactions of lanthanum ions hydroxylation were collected solely from the works of Kragten et al. [13] and were determined experimentally at room temperature in a perchlorate medium under a nitrogen atmosphere.

Table 1: Reaction constants used in this study (data sources: [13])

Reactions	Reaction constants
$La^{3+} + H_2O = La(OH)^{2+} + H^+$	$\beta_{1,1}^{*}=10^{-8.6}$
$La^{3+} + 2H_2O = La(OH)_2^{+} + 2H^+$	$\beta_{2,1}^{*}=10^{-17.9}$
$La^{3+} + 3H_2O = La(OH)_3 + 3H^+$	$\beta_{3,1}^{*}=10^{-27.3}$

La (IV) species were not considered in the speciation calculations because the equilibrium between trivalent and tetravalent lanthanum species is only observed under extreme oxidising conditions (see Fig. S1 in the supporting material file).

The total amount of lanthanum species in solution considered to build the speciation diagram presented in Fig. 2 did not exceed the maximum solubility of lanthanum hydroxide determined by Kragten and

Decnop-Weever [13]. Therefore, $La(OH)_{3\,(s)}$ species was not visible in the speciation diagram. Lanthanide polymeric hydrolysis species, whose existence has been hypothesised in several studies [18–24], were not considered. The reason for this is that there is significant uncertainty regarding the formation constants of these species [25,26]. More importantly, the goal of these thermodynamic calculations was to identify potential reactions that may affect surface lanthanide ions. Therefore, there was limited interest in implementing hydrolytic polymerisation reactions in the thermodynamic models. Because only a few studies have discussed the existence of $Ln(OH)_4^-$ species [27,28], this highly hydroxylated species was also excluded from this study.

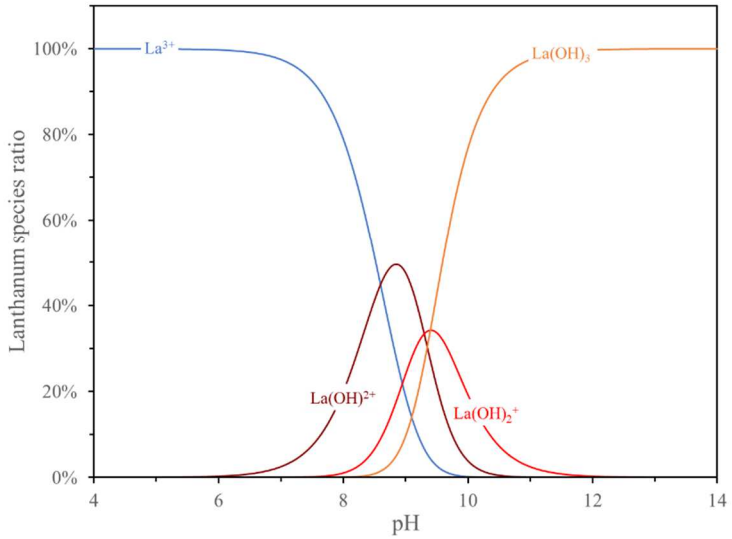

Figure 2: Speciation diagram of lanthanum species in aqueous solution. Total lanthanum concentration: 0.1 µM

3.2. Thermodynamic model of an H_2O-CO_2 system in equilibrium with $LaPO_{4\,(s)}$

The standard speciation model detailed in Section 3.1 indicates that under certain pH conditions, free lanthanide ions will be subjected to different extents of hydroxylation in the bulk. The assumptions regarding the effects of monazite surface speciation on flotation performance were based on the interpretation of basic models that only consider the hydroxylation of lanthanide ions. Because rare-earth elements are known to have a greater affinity for carbonate groups, rather than hydroxyl groups [13], lanthanide carbonate species should also be added to these thermodynamic models. In this context, a thermodynamic model for the dissolution of a monazite-(La) crystal in an H_2O/CO_2 system was developed. The reactions considered in this model are listed in Table 2. All

calculations were conducted assuming that 1) the amount of solid $LaPO_4$ in the solution is sufficient to avoid the limitation of the formation of subsequently formed species; 2) the system is open to the atmosphere, whose carbon dioxide concentration is considered to be 410 ppm ($pCO_2=10^{-3.39}$ atm); and 3) the Henry's law constant for CO_2 remains stable in the studied range of 4–14 pH, although the value considered is only valid for a salinity of zero [29]. Therefore, in the absence of any limiting reagents, the model reflects the influence of pH on monazite solubility and the concentration of lanthanide species in the bulk. It is important to note that, since published thermodynamic constants of lanthanide species are scarce and rarely extrapolated to infinite dilution, we used both standard and apparent thermodynamic constants in our calculations.

Equation (1), where K_{s0} represents the solubility product of monazite-(La), represents the evolution of the total lanthanum concentration in the bulk as a function of pH conditions. Based on the total lanthanum concentration, the concentrations of each lanthanum species were calculated. The results are presented in Fig. 3 to 6 in the form of aqueous species concentration diagrams indicating the chemistry of the equilibrated bulk solution and in the form of speciation diagrams indicating the predominant lanthanum species in the bulk solution. The figures indicate that free lanthanide species have a strong affinity for carbonate ions. As illustrated in Fig. 7, the complexation of lanthanide ions by carbonate ions significantly affects monazite-(La) solubility and the concentration of dissolved lanthanide species under alkaline conditions. It is likely that such high lanthanide carbonate species concentrations in the bulk are not possible and would induce the precipitation of lanthanide carbonate species, such as $La_2(CO_3)_3$. As discussed previously, in the case of hydrolytic polymerisation reactions, for the purposes of this study, there was no interest in implementing polynuclear species, such as lanthanum carbonates, in the thermodynamic model. In the case of lanthanum hydroxide species, their calculated concentrations in the bulk did not exceed the maximum lanthanum solubilities determined by Kragten and Decnop-Weever [13]. Therefore, the $La(OH)_{3\,(s)}$ species was not included in these diagrams.

$$[La^{3+}] = \sqrt{K_{s0} \times \frac{1+10^{12.4}[H^+]+10^{19.5}[H^+]^2+10^{21.7}[H^+]^3}{1+\left(\frac{10^{-8.6}}{[H^+]}+\frac{10^{-17.9}}{[H^+]^2}+\frac{10^{-27.3}}{[H^+]^3}\right)+\left(10^{-5.5}\times\frac{p_{CO_2}}{[H^+]}+10^{-11.4}\times\frac{p_{CO_2}}{[H^+]^2}+10^{-25.0}\times\frac{{p_{CO_2}}^2}{[H^+]^4}\right)}} \qquad \text{(eq. 1)}$$

Table 2: Equations for calculating the bulk chemistry at thermodynamic equilibrium

Equation	log(*K*)	Reference
$LaPO_{4\,(s)} = La^{3+}{}_{(aq)} + PO_4^{3-}{}_{(aq)}$	–25.7	[30]
$PO_4^{3-}{}_{(aq)} + H^+ = HPO_4^{2-}{}_{(aq)}$	12.35	[17]
$HPO_4^{2-}{}_{(aq)} + H^+ = H_2PO_4^-{}_{(aq)}$	7.198	[17]
$H_2PO_4^-{}_{(aq)} + H^+ = H_3PO_{4(aq)}$	2.148	[17]
$CO_{2\,(g)} + H_2O = H_2CO_{3\,(aq)}$	–1.469	[29]
$H_2CO_{3\,(aq)} = HCO_3^-{}_{(aq)} + H^+.$	–6.351	[31]
$HCO_3^-{}_{(aq)} = CO_3^{2-}{}_{(aq)} + H^+$	–10.330	[31]
$La^{3+}{}_{(aq)} + H_2O = La(OH)^{2+}{}_{(aq)} + H^+$	–8.55	[13]
$La(OH)^{2+}{}_{(aq)} + H_2O = La(OH)_2^+{}_{(aq)} + H^+$	–9.38	[13]
$La(OH)_2^+{}_{(aq)} + H_2O = La(OH)_{3(aq)} + H^+$	–9.38	[13]
$La^{3+}{}_{(aq)} + HPO_4^{2-}{}_{(aq)} = LaHPO_4^+{}_{(aq)}$	4.107	[32]
$La^{3+}{}_{(aq)} + H_2PO_4^-{}_{(aq)} = LaH_2PO_4^{2+}{}_{(aq)}$	1.787	[32]
$La^{3+}{}_{(aq)} + HCO_3^-{}_{(aq)} = LaHCO_3^{2+}{}_{(aq)} + H^+$	2.34	[33]
$La^{3+}{}_{(aq)} + CO_3^{2-}{}_{(aq)} = LaCO_3^+{}_{(aq)}$	6.73	[33]
$La^{3+}{}_{(aq)} + 2CO_3^{2-}{}_{(aq)} = La(CO_3)_2^-{}_{(aq)}$	11.30	[33]

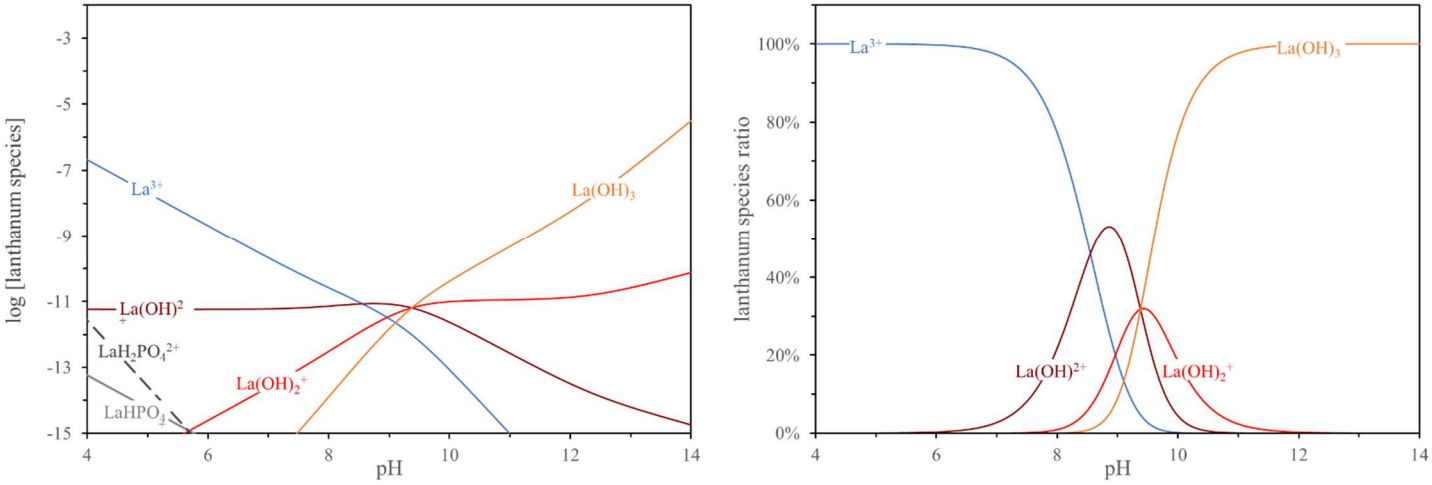

Figure 3: Lanthanum species concentrations (left) and related speciation diagram (right) in the case of an equilibrated monazite-(La)/H₂O system

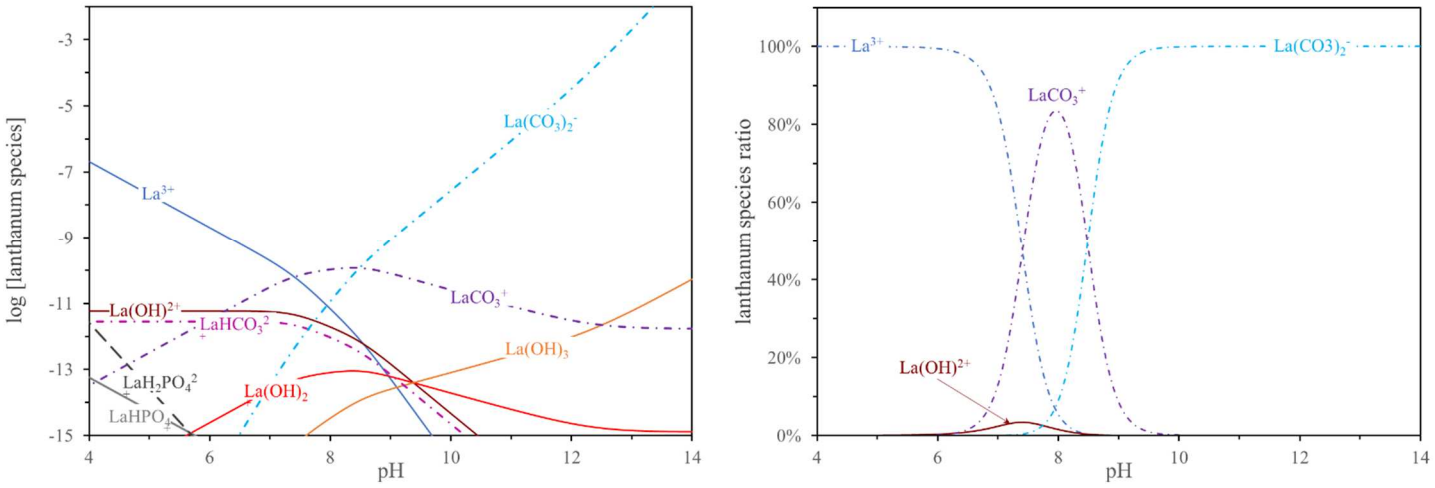

Figure 4: Lanthanum species concentrations (left) and related speciation diagram (right) in the case of an equilibrated monazite-(La)/H_2O-CO_2 system (open atmosphere)

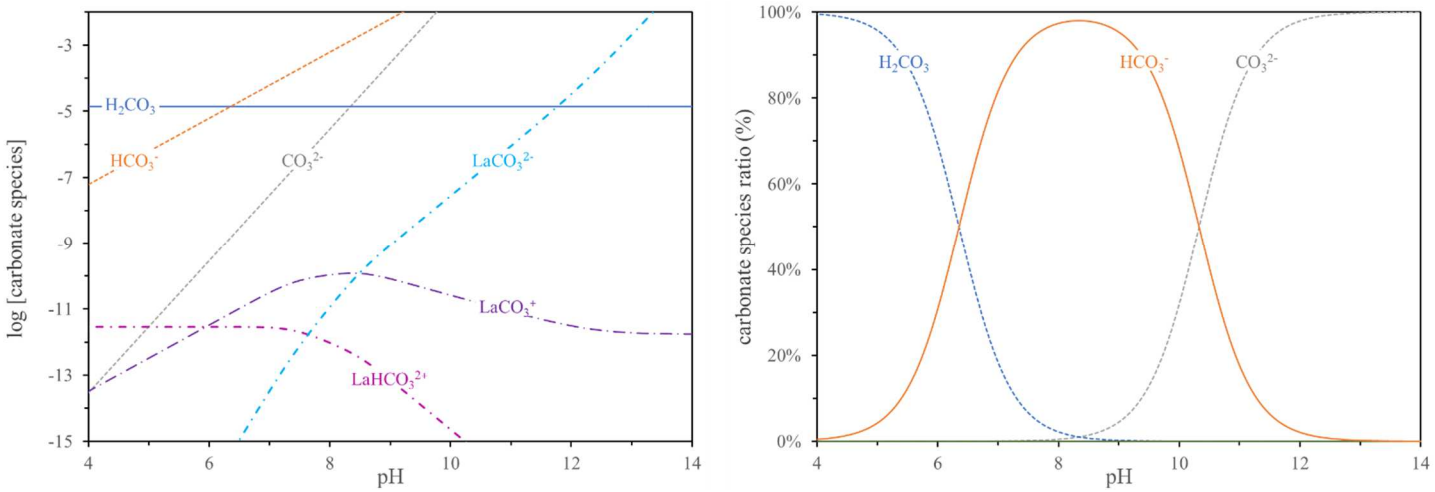

Figure 5: Carbonate species concentrations (left) and related speciation diagram (right) in the case of an equilibrated monazite-(La)/H_2O-CO_2 system (open atmosphere)

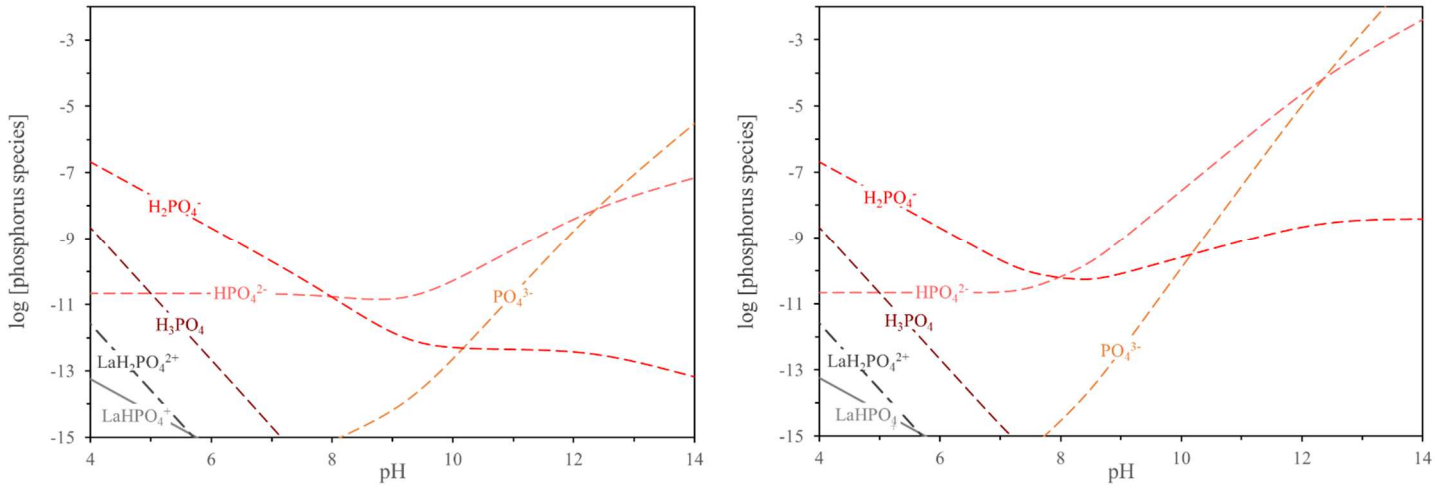

Figure 6: Phosphate species concentrations in the case of an equilibrated monazite-(La)/H_2O system (left) and monazite-(La)/H_2O-CO_2 system (open atmosphere) (right)

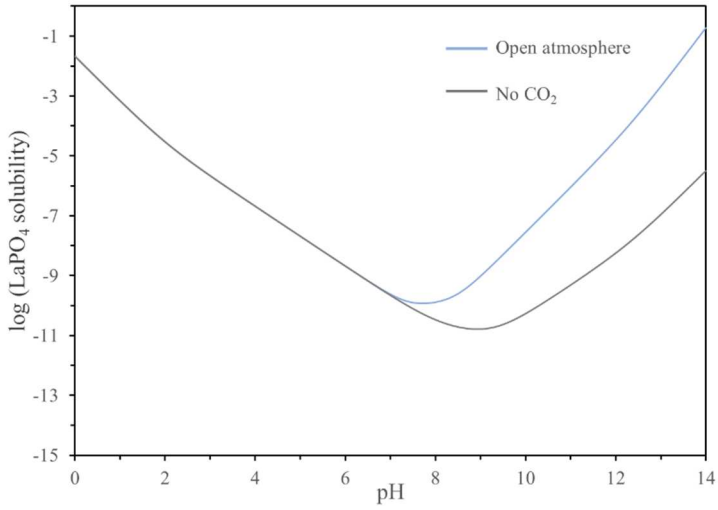

Figure 7: $LaPO_4$ solubility as a function of pH

4. Results and discussion

The structure of the monazite consists of an alternation of phosphate tetrahedrons and lanthanide enneaoxide polyhedrons. Monazite crystal cleavage occurs along the (100) plane, thereby exposing under-coordinated lanthanide polyhedrons to the solution. Considering the chemical stability of the phosphate tetrahedrons, it is likely that breakage of the crystal lattice will affect the lanthanide polyhedrons. A monazite slab with an exposed (100) facet was generated using the VESTA program [34]. This model is presented in Fig. 8. To make the model easier to read, the atomic radii were decreased by 50%. As shown in the 3D model, the lanthanide polyhedrons

exposed on the mineral surface are missing one or two of their nine oxygen sites. Based on this under-coordination, the lanthanide ions may form chemical bonds with water molecules, media species, and dissolved species to restore their nine-fold coordination shells. In the case of carbonate minerals, studies have shown that under-coordinated ions on such mineral surfaces may be subjected to reaction mechanisms similar to those affecting dissociated ions in the bulk [11,12]. In accordance with the previous thermodynamic calculations, it may be hypothesised that under appropriate pH conditions, surface lanthanide ions presenting vacant coordination sites will react with hydroxide or dissolved carbonate species to form hydroxylated or carbonated surface sites.

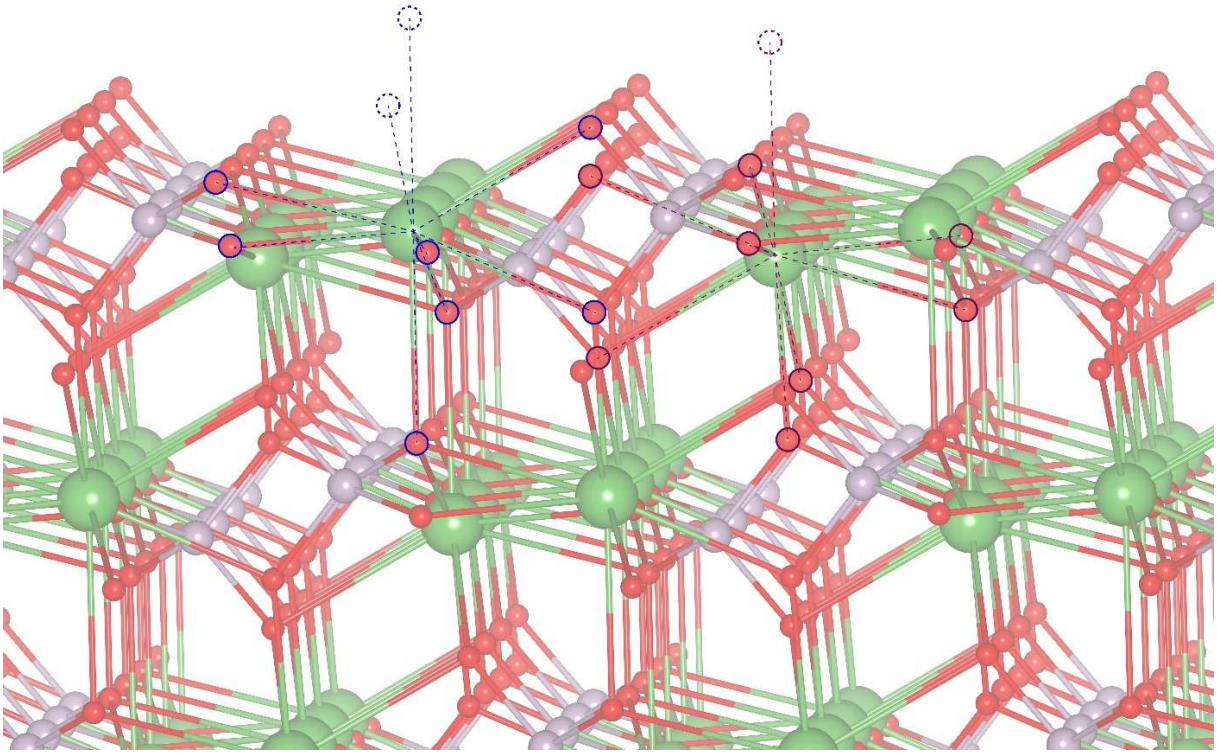

Figure 8: Ball-and-stick model of a monazite-(La) (100) facet with exposed truncated lanthanide enneaoxide polyhedrons (La: green, O: red, P: purple)

FTIR and XPS analyses were performed to assess the hydroxylation and carbonation of the under-coordinated surface lanthanide ions. As described in Section 2.1, it is important to note that the FTIR and XPS analyses were performed using different granular size fractions.

In order to determine the influence of pH on monazite surface speciation, a first series of FTIR analyses was

performed on monazite-(La) samples treated for 1 h under various pH conditions. The entire FTIR spectrum of the reference material is visible in Fig. 9 and is compared to the FTIR spectrum of the treated monazite in Fig. 10. The assignments of the different vibrational bands observed in the FTIR spectrum are listed in Table 3.

Table 3: Assignments of the different vibrational bands visible on the FTIR spectra of monazite-(La) presented in this study

Wavenumber (cm^{-1})	Vibration assignment	Source
625	$(P\text{-}O)_{asym.}$ bending	[35]
955	$(P\text{-}O)_{sym.}$ stretching	[35]
996	$(P\text{-}O)_{asym.}$ stretching	[35]
1034	$(P\text{-}O)_{asym.}$ stretching	[35]
1070	$(P\text{-}O)_{asym.}$ stretching	[35]
1092	$(P\text{-}O)_{asym.}$ stretching	[35]
1382	Carbonate asym. stretching	[36–38]
1458	Carbonate asym. stretching	[36,39,40]
1508	Carbonate asym. stretching	[41] [36]
1655	(O-H) bending	[42,43]

Absorbance band characteristics of the phosphate groups in the lanthanide phosphates [35,44,45] were observed at 625 cm^{-1}, 955 cm^{-1}, 996 cm^{-1}, 1034 cm^{-1}, 1070 cm^{-1}, and 1092 cm^{-1}. The first and second harmonics of the fundamental bands of the symmetrical stretching vibrations of the phosphate groups were also observed and are visible in Fig. 9. These harmonic bands, which are not reported in the literature, were likely detected because of the higher sensitivity to low-intensity absorbance bands of the DRIFT vibrational spectroscopy technique.

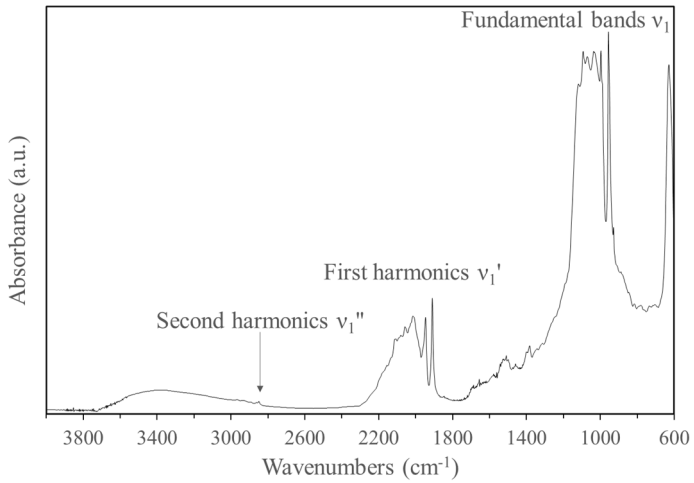

Figure 9: FTIR spectrum of the synthetic monazite-(La) reference sample

The FTIR spectrum of synthetic $La(OH)_3$ showed a sharp band at 3609 cm^{-1} corresponding to a hydroxyl group linked to La^{3+} ions [36,46,47]. None of the monazite-(La) spectra presented in Fig. 10 show such an absorbance peak. However, considering that hydroxylation is a mechanism only affecting surface lanthanide ions exposed to the solution, only minor peaks were expected. Therefore, it is difficult to detect this peak because of the stretching vibrations of the hydroxyl groups of molecular water, which generates a large absorbance anomaly at approximately 3400 cm^{-1} [38,42,47]. The minor absorbance peak at approximately 1655 cm^{-1} has already been reported in the literature in the cases of several rare-earth materials and is attributed to the bending vibrations of the hydroxyl groups of molecular water [42,43]. In comparison with the reference sample, the intensity of the absorbance band at 1655 cm^{-1} is increased after treating the monazite under various pH conditions. The absence of influence of the treatment pH conditions on the intensity of this absorbance band possibly betrays the presence of remaining water or adsorbed molecular water. Therefore, there is no absorbance band that can be attributed to a mineral surface hydroxylation or, more importantly, that can be used to study the influence of treatment pH conditions on the extent of surface hydroxylation.

Different absorbance bands in the region of 1380–1508 cm^{-1} were attributed to the asymmetric stretching of carbonate groups, confirming that the monazite surface may carbonate. However, the intensity of these absorbance bands is not significantly affected by pH conditions during treatment. There are two possible

interpretations of this phenomenon. First, under the experimental conditions, the kinetics of carbonation of the monazite-(La) surface may have been too weak to observe a change in the FTIR spectra. Second, the surface carbonation may have already reached its maximum extent during sample preparation (manual crushing and wet sieving). A second series of experiments was performed with monazite-(La) treated for 1 h in a solution containing 10 wt% Na_2CO_3 to promote further carbonation of the mineral surface. The FTIR spectra of the treated monazite are compared to that of the reference material in Fig. 11. It is important to note that the amount of dissolved carbonate species in the solution at pH 8.9 was lower than at pH 11 based on the significant CO_2 degassing that occurs during pH adjustment. A slight increase in the intensity of the band at 1508 $cm^{-1}$was observed when treating monazite-(La) grains with Na_2CO_3 at pH 11, although it is not sufficiently significant to conclude that the monazite surface may undergo further carbonation under alkaline pH conditions. Therefore, after 1 h of treatment, it is difficult to reach solid conclusions regarding the ability of surface lanthanide ions to interact with carbonate groups and the effect of pH conditions on mineral surface carbonation.

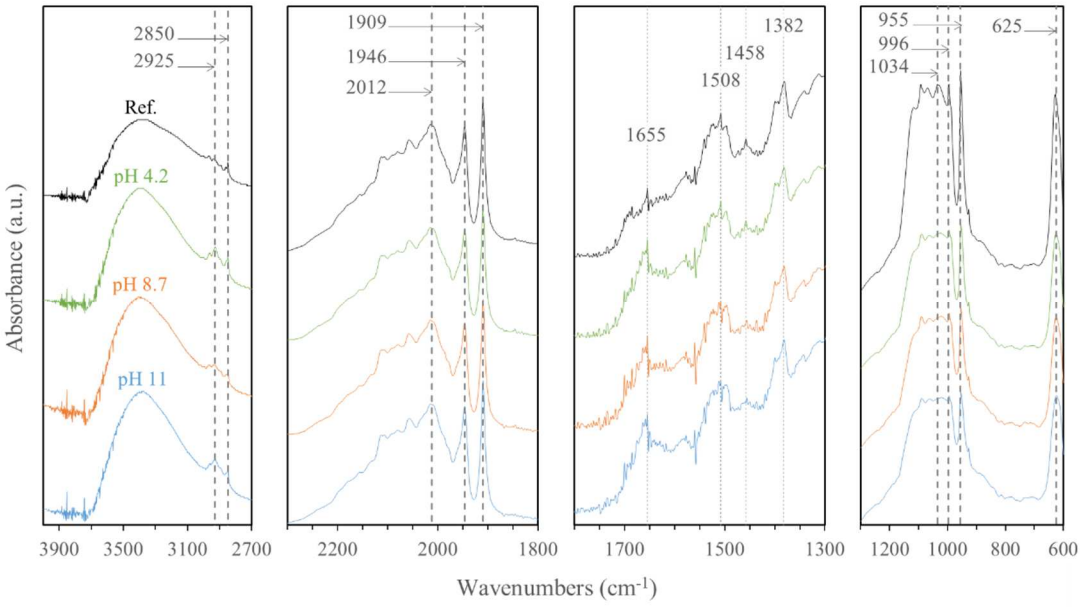

Figure 10: FTIR spectra of synthetic monazite-(La) treated with deionised water under different pH conditions

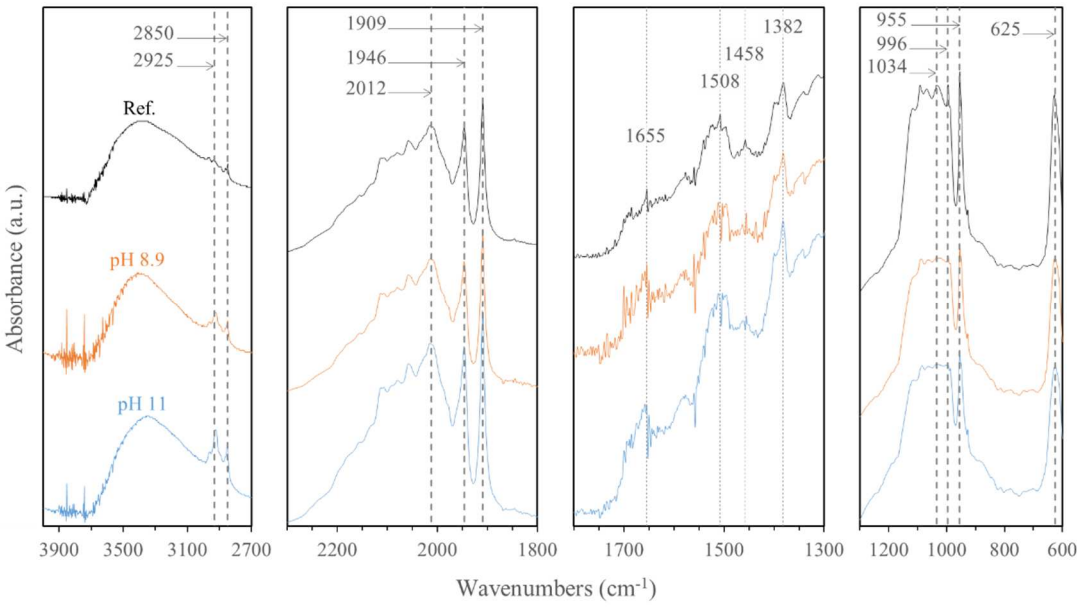

Figure 11: FTIR spectra of synthetic monazite-(La) treated with deionised water and Na_2CO_3 under different pH conditions

Based on the difficulty in assigning the hydroxylation of the monazite surface within the FTIR spectra, a series of XPS analyses were performed on monazite-(La) treated under various pH conditions. The treatment of the monazite powder was performed in a closed atmosphere using test tubes. The deionised water was initially equilibrated with the air and the pH was adjusted to the desired value. The monazite powder was then added and the suspensions were mixed for 1 h in a laboratory shaker. The high-resolution XPS La 3d and O 1s core level spectra presented in Fig. 12 were normalised in intensity to assess eventual binding energy shifting. It is important to note that the pH mentioned in this figure is the equilibrium pH which was measured at the end of the monazite treatment. No significant differences can be observed between the spectra of the reference sample and those of the treated monazite powders. The observation or decomposition of the La 3d and O 1s spectra alone cannot provide a comprehensive assessment of monazite surface hydroxylation.

In the high-resolution XPS La 3d core level spectra of several lanthanum materials reported in the literature, the binding energy separation between the main and satellite peaks (spin-orbit splitting) differs significantly from one lanthanum material to another [48]. However, the observed magnitude of the spin-orbit splitting (ΔE = 3.6 eV) of the reference $LaPO_4$ sample is very close to that reported for $La(OH)_3$ component [47,49]. Therefore, it is uncertain whether or not the spin-orbit splitting of the La 3d spectra can assist in the assessment

of lanthanum phosphate surface hydroxylation. Furthermore, the binding energy of the oxygen from the surface lanthanide hydroxides (frequently assigned at 531.2 eV [50,51] or 531.9 eV [52]) and that of the oxygen from the lattice phosphate group in a $LaPO_4$ structure (assigned at 531.6 eV [53]) are indistinguishable. Therefore, the decomposition of the high-resolution XPS O 1s core level spectra cannot be used to assess monazite surface hydroxylation.

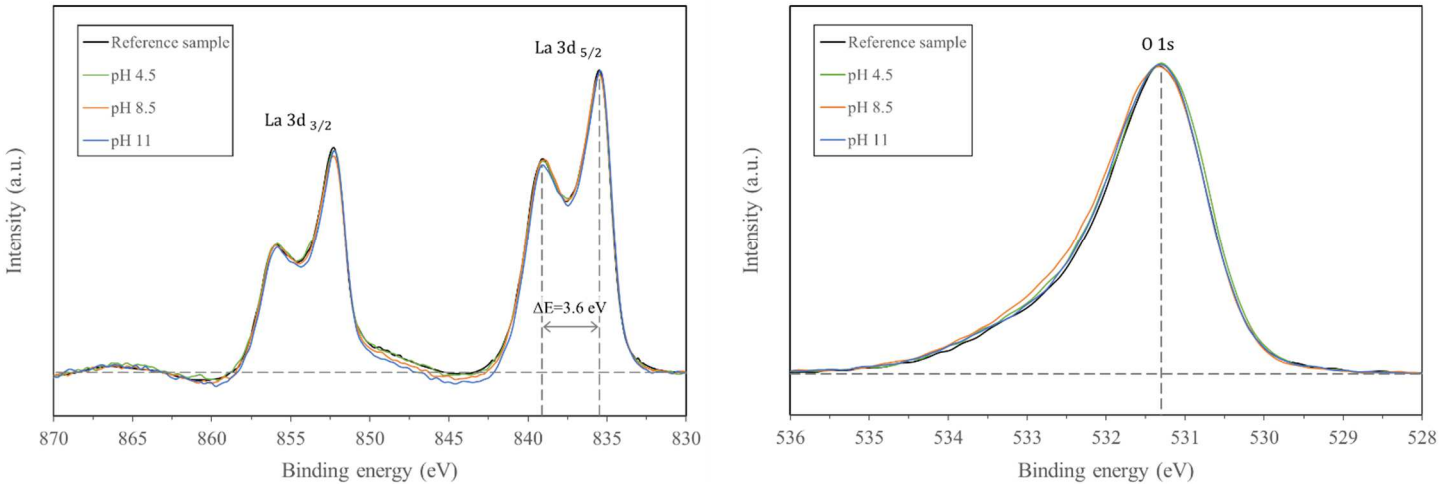

Figure 12: High-resolution XPS La 3d (left) and O 1s (right) core level spectra of monazite-(La) treated under various pH conditions. Note that the spectra were normalised in intensity

In contrast to the FTIR analyses, the XPS analyses were carried out under an ultra-high vacuum, comparatively limiting the amounts of remaining or adsorbed molecular water. Therefore, the oxygen-to-lanthanum surface atomic ratio should be used to assess the hydroxylation of the surface lanthanide ions. The phosphorus-to-lanthanum and oxygen-to-lanthanum surface atomic ratios are listed in Table 4. We found that when increasing the pH level, while the phosphorus-to-lanthanum atomic ratio remained equal to the standard ratio of 1:1, the oxygen-to-lanthanum atomic ratio seems to increase. However, mineral surface carbonation and the presence of carbonaceous components (adventitious carbon) on the mineral surface induced a relative oxygen overdose. In order to calculate an oxygen-to-lanthanum atomic ratio which do not includes the contributions of the adventitious carbon and adsorbed carbonate groups to the total oxygen content, the amount of C-O and CO_3^{2-} on the mineral surface were back-calculated by decomposition of the high-resolution XPS C 1s core level spectra presented in Fig. 13 into three components, namely C-(C,H), C-O, and CO_3^{2-}. After subtracting these contributions, the corrected oxygen-to-lanthanum ratio was affected only by the hydroxide or phosphate groups.

The corrected atomic ratio was found equal to 4.0 for the reference sample, which is consistent with the lanthanum phosphate composition. Although an acidic treatment does not affect this ratio, an alkaline treatment seems to increase it, which mirrors the effect of pH on the hydroxylation of free lanthanide ions in the bulk, which was discussed in Section 3.2.

The commonly referenced mechanism for monazite surface activation by hydroxylated lanthanide ions involves the dissociation of crystal lattice species, hydrolysis of dissolved lanthanide species under certain pH conditions, and specific re-adsorption of lanthanide hydroxides on the mineral surface [4]. The series of XPS analyses on monazite-(La) samples treated at different pH levels indicates a lanthanum-to-phosphorus atomic ratio close to one. This represents a strong argument against the mechanism of rare-earth semi-soluble salt surface hydroxylation. It is more likely that the hydroxylation of the monazite surface occurs via direct hydrolysis of under-coordinated surface lanthanide ions.

Table 4: Effects of pH conditions on the XPS-derived atomic ratios of monazite-(La) samples treated under various pH conditions

Atomic ratio	pH conditions			
	Reference	4.5	8.5	11
phosphorus-to-lanthanum	1.0	1.0	1.0	1.0
oxygen-to-lanthanum	4.3	4.4	4.8	4.9
corrected oxygen-to-lanthanum	4.0	3.9	4.4	4.6

The series of XPS analyses of monazite-(La) also provided information regarding mineral surface carbonation. The presence of carbonate species on the mineral surface should result in a photoelectron emission whose binding energy is approximately 288.2 eV in the case of lanthanum materials [54,55]. This photoelectron emission can be distinguished from the photoelectron emissions assigned to the C-(C, H) bonds at approximately 284.6 eV and C-O bond at approximately 286 eV [56] in the adventitious carbon. The intensity normalised high-resolution XPS

C 1s core level spectra of the reference monazite sample and treated samples are represented in Fig. 13. An insignificant photoelectron emission corresponding to carbonate species can be observed for each sample. The identical C 1s spectra for all treated materials and the reference material confirm the absence of mineral surface carbonation during treatment.

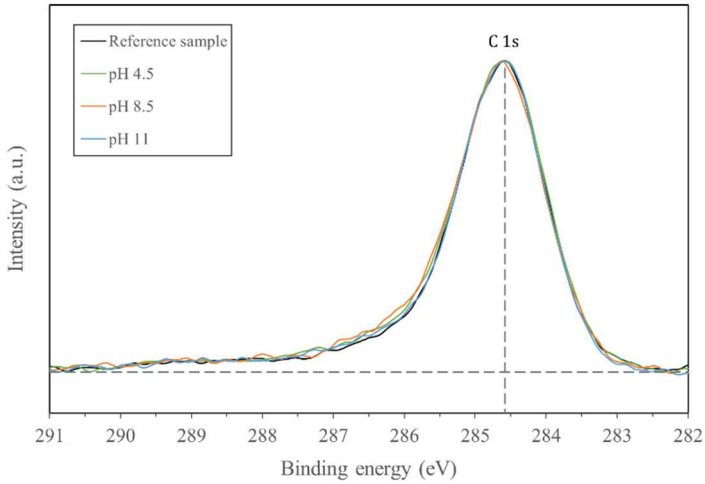

Figure 13: High-resolution XPS C 1s core level spectra of monazite-(La) treated under various pH conditions. Note that the spectra were normalised in intensity

To determine if a treatment in the presence of Na_2CO_3 results in further surface carbonation, samples of the same monazite-(La) powder were mixed for 1 h in an open beaker containing 35 mL of a sodium carbonate solution (1 and 10 wt% Na_2CO_3). During this treatment, the pH of the suspensions remains stable and equal to 11.5–11.7. A thorough rinsing with deionised water was performed to avoid any precipitation of remaining sodium carbonate and solely detect the carbonate species adsorbed on the mineral surface. The high-resolution XPS C 1s and Na 1s core level spectra of the treated sample and initial powder are presented in Fig. 14. No significant increase in the amount of carbonate species on the mineral surface can be observed after treatment with sodium carbonate. Therefore, it can be concluded that either no carbonation of the mineral occurred or the interaction of the surface lanthanide ions with dissolved carbonate species is too weak to avoid a carbonate species desorption during thorough rinsing with deionised water.

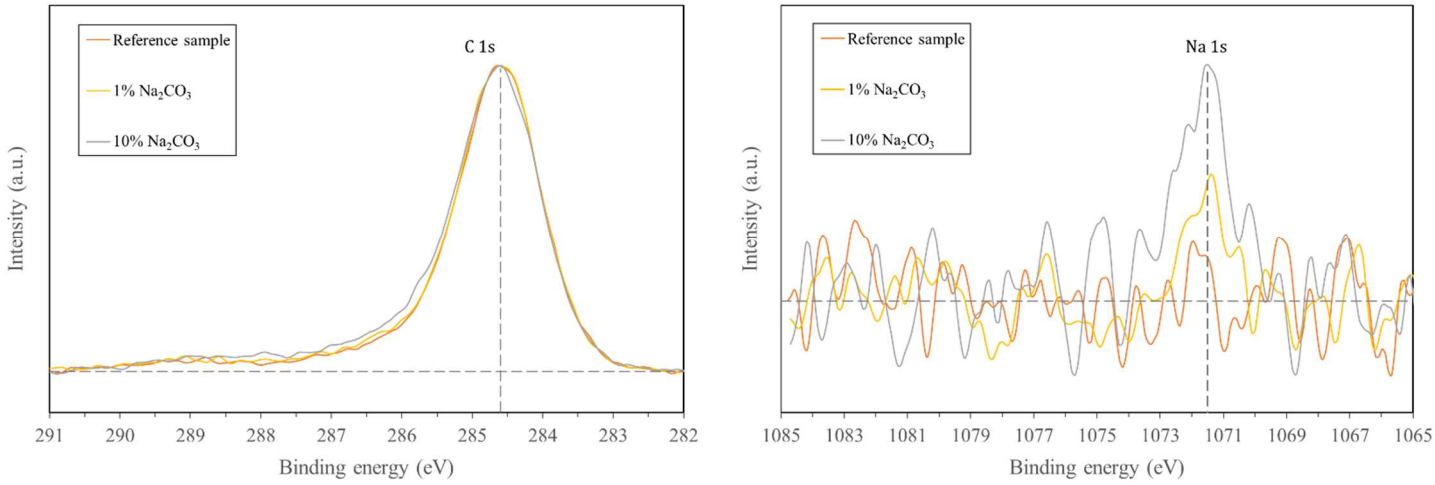

Figure 14: High-resolution XPS C 1s (left) and Na 1s (right) core level spectra of monazite-(La) treated under various Na_2CO_3 concentrations. Note that only the C 1s core level spectra were normalised in intensity

The FTIR analyses suggest that the slight carbonation observed on the surface of the monazite samples appeared before the treatment under different pH conditions. Even a treatment in sodium carbonate solutions did not result in a significant increase in the intensity of the FTIR absorbance bands assigned to the carbonate stretching or a significant increase in the carbonate species X-ray photoelectron emissions measured via XPS. Although the monazite surface was reported to have no strong interaction with the carbonate species, hydroxylation of the mineral surface is suspected under alkaline conditions based on the XPS analyses. These monazite surface probing results are inconsistent with the thermodynamic data regarding the speciation of free lanthanide ions in the bulk. However, as illustrated in Fig. 8, the truncated Ln (III) polyhedrons exposed on the cleaved mineral surface are only missing one or two of their nine coordination sites, which may result in one-third or two-thirds of an elementary positive charge. This means that the reactivity of the surface lanthanide ions with the hydroxide and carbonate groups is limited and they are unlikely to undergo the same extent of hydroxylation or carbonation as when they are free in the bulk.

5. Conclusions

This study focused on the assessment of the speciation of lanthanide ions on monazite surface. In this context, a model of mineral/aqueous solution thermodynamic equilibrium was proposed. The main innovation of this model is the consideration of the carbonation of lanthanide ions in the solution. From a thermodynamic

perspective, this model highlights the fact that free lanthanide ions in the bulk will hydroxylate or carbonate under alkaline conditions. In a system open to the atmosphere, the complexation of lanthanide ions by carbonate groups is thermodynamically favoured over complexation by hydroxyl groups. It was shown that the surface lanthanide ions present on the (100) main cleavage plane are under-coordinated and present one or two vacant sites. Therefore, under appropriate conditions, it is suspected that they undergo hydroxylation and carbonation reactions to restore their nine-fold coordination shells.

The atomic ratios determined by the XPS analyses seem to suggest that surface lanthanide ions hydroxylate under alkaline conditions. However, considering that the truncated lanthanide polyhedrons exposed on the mineral surface were only missing one or two of their nine coordination sites, the surface lanthanide ions will not undergo the same extent of hydroxylation as the free lanthanide ions in the bulk. Under the test conditions, the surface lanthanide ions were also reported to interact more with hydroxyl ions than with dissolved carbonate species. These results are inconsistent with the thermodynamic data and confirm that the reactivities of free lanthanide ions and surface lanthanide ions with carbonate species are not comparable.

Finally, our assessment of surface lanthanide ion speciation offers an excellent basis for the study of the mechanisms of adsorption of carboxylate collectors onto monazite surface. This subject will be discussed in the second part of this series.

Acknowledgements

This research was funded by the Carnot Institutes ICEEL and BRGM through the TERRAFINE Inter-Carnot Action (Carnot-ICEEL no. 118-IC and IC-BRGM no. 2013-01). Financial support from LabEx RESSOURCES21 is also acknowledged (contract Investissements d'Avenir no. ANR–10–LABX–0021).

The authors would like to thank Odile Barres (GeoRessources) for her expertise in FTIR spectroscopy and Pierric Hubert (GeoRessources) for his assistance with XRD analysis.

References

[1] N. Krishnamurthy, C. Gupta, Extractive metallurgy of rare earths, Second edition, CRC Press, Boca Raton,

2016.

[2] C.J. Ferron, S.M. Bulatovic, R.S. Salter, Beneficiation of Rare Earth Oxide Minerals, Mater. Sci. Forum. 70–72 (1991) 251–270. doi:10.4028/www.scientific.net/MSF.70-72.251.

[3] A. Jordens, The beneficiation of rare earth element-bearing minerals, PhD Thesis, Department of Mining and Materials Engineering, McGill University, 2016.

[4] Pradip, D.W. Fuerstenau, The adsorption of hydroxamate on semi-soluble minerals. Part I: Adsorption on barite, Calcite and Bastnaesite, Colloids Surf. 8 (1983) 103–119. doi:10.1016/0166-6622(83)80079-1.

[5] T.-W. Cheng, P.N. Holtham, T. Tran, Froth flotation of monazite and xenotime, Miner. Eng. 6 (1993) 341–351. doi:10.1016/0892-6875(93)90014-E.

[6] W. Zhang, R. Honaker, A fundamental study of octanohydroxamic acid adsorption on monazite surfaces, Int. J. Miner. Process. 164 (2017) 26–36. doi:10.1016/j.minpro.2017.05.006.

[7] T.-W. Cheng, A.C. Partridge, T. Tran, P.L.M. Wong, The surface properties and flotation behaviour of xenotime, Miner. Eng. 7 (1994) 1085–1098. doi:10.1016/0892-6875(94)90001-9.

[8] E.R.L. Espiritu, S. Naseri, K.E. Waters, Surface chemistry and flotation behavior of dolomite, monazite and bastnäsite in the presence of benzohydroxamate, sodium oleate and phosphoric acid ester collectors, Colloids Surf. Physicochem. Eng. Asp. 546 (2018) 254–265. doi:10.1016/j.colsurfa.2018.03.030.

[9] Z. Yang, Synthesis of 3-hydroxy-2-naphthyl hydroxamic acid collector: flotation performance and adsorption mechanism on bastnaesite, J. South. Afr. Inst. Min. Metall. 117 (2017) 593–598. doi:10.17159/2411-9717/2017/v117n6a10.

[10] E.R.L. Espiritu, K.E. Waters, Flotation studies of monazite and dolomite, Miner. Eng. 116 (2018) 101–106. doi:10.1016/j.mineng.2017.02.010.

[11] P. Van Cappellen, L. Charlet, W. Stumm, P. Wersin, A surface complexation model of the carbonate mineral-aqueous solution interface, Geochim. Cosmochim. Acta. 57 (1993) 3505–3518. doi:10.1016/0016-7037(93)90135-J.

[12] O.S. Pokrovsky, J.A. Mielczarski, O. Barres, J. Schott, Surface Speciation Models of Calcite and Dolomite/Aqueous Solution Interfaces and Their Spectroscopic Evaluation, Langmuir. 16 (2000) 2677–2688. doi:10.1021/la980905e.

[13] J. Kragten, L.G. Decnop-Weever, Hydroxide complexes of lanthanides-VIII: lanthanum(III) in perchlorate medium, Talanta. 34 (1987) 861–864. doi:10.1016/0039-9140(87)80115-7.

[14] A. Geneyton, L.O. Filippov, N.. Menad, Effects of atom substitutions and dissolved carbonate species on monazite electrophoretic mobility, Colloids Surf. Physicochem. Eng. Asp. 570 (2019) 141–146. doi:10.1016/j.colsurfa.2019.03.005.

[15] A. Sarvaramini, D. Azizi, F. Larachi, Hydroxamic acid interactions with solvated cerium hydroxides in the flotation of monazite and bastnäsite—Experiments and DFT study, Appl. Surf. Sci. 387 (2016) 986–995. doi:10.1016/j.apsusc.2016.07.044.

[16] S.A. Hayes, P. Yu, T.J. O'Keefe, M.J. O'Keefe, J.O. Stoffer, The Phase Stability of Cerium Species in Aqueous Systems, J. Electrochem. Soc. 149 (2002) C623. doi:10.1149/1.1516775.

[17] D.R. Lide, CRC Handbook of Chemistry and Physics, 85th ed., CRC Press, Boca Raton, Florida, USA, 2005.

[18] J. Kragten, Hydroxide complexes of cerium(III), Talanta. 25 (1978) 147–150. doi:10.1016/0039-9140(78)80103-9.

[19] J. Kragten, L.G. Decnop-Weever, Hydroxide complexes of lanthanides-VII: neodymium(III) in perchlorate medium, Talanta. 31 (1984) 731–733. doi:10.1016/0039-9140(84)80161-7.

[20] E. Furia, R. Porto, 2-Hydroxybenzamide as a Ligand. Complex Formation with Dioxouranium(VI), Aluminum(III), Neodymium(III), and Nickel(II) Ions, J. Chem. Eng. Data. 53 (2008) 2739–2745. doi:10.1021/je800142f.

[21] L. Ciavatta, R. Porto, E. Vasca, The hydrolysis of the cerium(III) ion, Ce^{3+}, in aqueous perchlorate solutions at 50 °C, Polyhedron. 7 (1988) 1355–1361. doi:10.1016/S0277-5387(00)80385-X.

[22] L. Ciavatta, R. Porto, E. Vasca, The hydrolysis of the neodymium(III) ion, nd3+, in3 m (Li) clo4 medium at 60 °C, Polyhedron. 8 (1989) 2701–2707. doi:10.1016/S0277-5387(00)80442-8.

[23] K.A. Burkov, L.S. Lilich, Nguen Dinh Ngo, A.Y. Smirnov, Potentiometric study of the hydrolysis of neodymium ions (Nd^{3+}) in 3 M (Na)ClO_4 solution, Russ J Inorg Chem. 18 (1973) 787–800.

[24] Q. Luo, Studies on hydrolytic polymerization of rare-earth metal ions—V Hydrolytic polymerization of Dy^{3+}, Talanta. 37 (1990) 357–360. doi:10.1016/0039-9140(90)80067-P.

[25] P.L. Brown, C. Ekberg, Hydrolysis of metal ions, Wiley-VCH Verlag GmbH & Co. KGaA, Weinheim, 2016.

[26] E. Vasca, D. Ferri, C. Manfredi, F. Fantasma, T. Caruso, C. Fontanella, S. Vero, On the hydrolysis of the Dysprosium(III) ion, Chem. Speciat. Bioavailab. 16 (2004) 71–77. doi:10.3184/095422904782775135.

[27] C.F. Baes, R.S. Mesmer, The hydrolysis of cations, John Wiley & sons, New York, London, Sydney, Toronto, 1976.

[28] D.. Turner, M. Whitfield, A.. Dickson, The equilibrium speciation of dissolved components in freshwater and sea water at 25 °C and 1 atm pressure, Geochim. Cosmochim. Acta. 45 (1981) 855–881. doi:10.1016/0016-7037(81)90115-0.

[29] R.F. Weiss, Carbon dioxide in water and seawater: the solubility of a non-ideal gas, Mar. Chem. 2 (1974) 203–215. doi:10.1016/0304-4203(74)90015-2.

[30] Z.S. Cetiner, S.A. Wood, C.H. Gammons, The aqueous geochemistry of the rare earth elements. Part XIV. The solubility of rare earth element phosphates from 23 to 150 °C, Chem. Geol. 217 (2005) 147–169. doi:10.1016/j.chemgeo.2005.01.001.

[31] F.J. Millero, T.B. Graham, F. Huang, H. Bustos-Serrano, D. Pierrot, Dissociation constants of carbonic acid in seawater as a function of salinity and temperature, Mar. Chem. 100 (2006) 80–94. doi:10.1016/j.marchem.2005.12.001.

[32] X. Liu, R.H. Byrne, Rare earth and yttrium phosphate solubilities in aqueous solution, Geochim. Cosmochim. Acta. 61 (1997) 1625–1633. doi:10.1016/S0016-7037(97)00037-9.

[33] Y.-R. Luo, R.H. Byrne, Carbonate complexation of yttrium and the rare earth elements in natural waters, Geochim. Cosmochim. Acta. 68 (2004) 691–699. doi:10.1016/S0016-7037(03)00495-2.

[34] K. Momma, F. Izumi, *VESTA 3* for three-dimensional visualization of crystal, volumetric and morphology data, J. Appl. Crystallogr. 44 (2011) 1272–1276. doi:10.1107/S0021889811038970.

[35] L. Macalik, P.E. Tomaszewski, A. Matraszek, I. Szczygieł, P. Solarz, P. Godlewska, M. Sobczyk, J. Hanuza, Optical and structural characterisation of pure and Pr^{3+} doped $LaPO_4$ and $CePO_4$ nanocrystals, J. Alloys Compd. 509 (2011) 7458–7465. doi:10.1016/j.jallcom.2011.04.077.

[36] B.P. Gangwar, V. Palakollu, A. Singh, S. Kanvah, S. Sharma, Combustion synthesized La_2O_3 and $La(OH)_3$:

recyclable catalytic activity towards Knoevenagel and Hantzsch reactions, RSC Adv. 4 (2014) 55407–55416. doi:10.1039/C4RA08353A.

[37] O.V. Manoilova, S.G. Podkolzin, B. Tope, J. Lercher, E.E. Stangland, J.-M. Goupil, B.M. Weckhuysen, Surface Acidity and Basicity of La_2O_3 , LaOCl, and $LaCl_3$ Characterized by IR Spectroscopy, TPD, and DFT Calculations, J. Phys. Chem. B. 108 (2004) 15770–15781. doi:10.1021/jp040311m.

[38] P. Jeevanandam, Y. Koltypin, O. Palchik, A. Gedanken, Synthesis of morphologically controlled lanthanum carbonate particles using ultrasound irradiation, J. Mater. Chem. 11 (2001) 869–873. doi:10.1039/b007370i.

[39] F. Ren, Y. Ding, Y. Leng, Infrared spectroscopic characterization of carbonated apatite: A combined experimental and computational study: Ir Spectroscopic Characterization of CAp, J. Biomed. Mater. Res. A. 102 (2014) 496–505. doi:10.1002/jbm.a.34720.

[40] B. Vallina, J.D. Rodriguez-Blanco, A.P. Brown, J.A. Blanco, L.G. Benning, The role of amorphous precursors in the crystallization of La and Nd carbonates, Nanoscale. 7 (2015) 12166–12179. doi:10.1039/C5NR01497B.

[41] C.E. Silva, L.P. Silva, H.G.M. Edwards, L.F.C. de Oliveira, Diffuse reflection FTIR spectral database of dyes and pigments, Anal. Bioanal. Chem. 386 (2006) 2183–2191. doi:10.1007/s00216-006-0865-8.

[42] J. Han, L. Wang, S.S. Wong, Observation of Photoinduced Charge Transfer in Novel Luminescent CdSe Quantum Dot–$CePO_4$:Tb Metal Oxide Nanowire Composite Heterostructures, J. Phys. Chem. C. 118 (2014) 5671–5682. doi:10.1021/jp4113816.

[43] F. Khosrow-pour, M. Aghazadeh, B. Sabour, S. Dalvand, Large-scale synthesis of uniform lanthanum oxide nanowires via template-free deposition followed by heat-treatment, Ceram. Int. 39 (2013) 9491–9498. doi:10.1016/j.ceramint.2013.05.067.

[44] B. Qian, S. Yang, X. Liang, Y. Lai, L. Gao, G. Yin, Structural and thermal properties of La_2O_3–Fe_2O_3–P_2O_5 glasses, J. Mol. Struct. 1011 (2012) 153–157. doi:10.1016/j.molstruc.2011.12.014.

[45] L. Ma, W.-X. Chen, Y.-F. Zheng, Z.-D. Xu, Hydrothermal growth and morphology evolution of $CePO_4$ aggregates by a complexing method, Mater. Res. Bull. 43 (2008) 2840–2849. doi:10.1016/j.materresbull.2008.01.002.

[46] S. Xin, L. Wang, H. Li, K. Huang, F. Li, Synthesis of diethyl carbonate from urea and ethanol over

lanthanum oxide as a heterogeneous basic catalyst, Fuel Process. Technol. 126 (2014) 453–459. doi:10.1016/j.fuproc.2014.05.029.

[47] A.B. Yousaf, M. Imran, M. Farooq, P. Kasak, Interfacial Phenomenon and Nanostructural Enhancements in Palladium Loaded Lanthanum Hydroxide Nanorods for Heterogeneous Catalytic Applications, Sci. Rep. 8 (2018). doi:10.1038/s41598-018-22800-0.

[48] H.C. Siegmann, L. Schlapbach, C.R. Brundle, Self-Restoring of the Active Surface in the Hydrogen Sponge La Ni 5, Phys. Rev. Lett. 40 (1978) 972–975. doi:10.1103/PhysRevLett.40.972.

[49] M.F. Sunding, K. Hadidi, S. Diplas, O.M. Løvvik, T.E. Norby, A.E. Gunnæs, XPS characterisation of in situ treated lanthanum oxide and hydroxide using tailored charge referencing and peak fitting procedures, J. Electron Spectrosc. Relat. Phenom. 184 (2011) 399–409. doi:10.1016/j.elspec.2011.04.002.

[50] V. Bondarenka, XPS study of epitaxial $LaNiO_{3-x}$ films, Lith. J. Phys. 46 (2006) 95–99. doi:10.3952/lithjphys.46114.

[51] A. Uhart, J.B. Ledeuil, D. Gonbeau, J.C. Dupin, J.P. Bonino, F. Ansart, J. Esteban, An Auger and XPS survey of cerium active corrosion protection for AA2024-T3 aluminum alloy, Appl. Surf. Sci. 390 (2016) 751–759. doi:10.1016/j.apsusc.2016.08.170.

[52] Y.-G. Cho, K.-H. Choi, Y.-R. Kim, J.-S. Jung, S.-H. Lee, Characterization and Catalytic Properties of Surface La-rich $LaFeO_3$ Perovskite, Bull. Korean Chem. Soc. 30 (2009) 1368–1372. doi:10.5012/bkcs.2009.30.6.1368.

[53] O. Ivanova, A. Naumkin, L. Vasilyev, An XPS study of compositional changes induced by argon ion bombardment of the LaPO4 surface, Vacuum. 47 (1996) 67–71. doi:10.1016/0042-207X(95)00180-8.

[54] G. Chen, B. Han, S. Deng, Y. Wang, Y. Wang, Lanthanum Dioxide Carbonate $La_2O_2CO_3$ Nanorods as a Sensing Material for Chemoresistive CO_2 Gas Sensor, Electrochimica Acta. 127 (2014) 355–361. doi:10.1016/j.electacta.2014.02.075.

[55] V.G. Milt, R. Spretz, M.A. Ulla, E.A. Lombardo, J.L.G. Fierro, The nature of active sites for the oxidation of methane on La-based perovskites, Catal. Lett. 42 (1996) 57–63. doi:10.1007/BF00814467.

[56] G. Beamson, D. Briggs, High Resolution XPS of Organic Polymers: The Scienta ESCA300 Database, Wiley, 1992.

s

Supporting material

Advances in carboxylate collector adsorption on monazite surface:

Part 1 – Assessment of the hydroxylation and carbonation of surface lanthanide ions

A. Geneyton [a,b], L.O. Filippov [a,*], A. Renard [c], M. Mallet [c], N.-E Menad [b]

[a] Université de Lorraine, CNRS, GeoRessources, F- 54000 Nancy, France
[b] D3E/DMP, Bureau de Recherche Géologique et Minière (BRGM), 3, Avenue Claude Guillemin, 45060, Orléans, France
[c] Université de Lorraine, CNRS, LCPME, F- 54000 Nancy, France

*Corresponding author: lev.filippov@univ-lorraine.fr, +33 3 72 74 45 46, 2 rue du Doyen Marcel Roubault, 54500, Vandoeuvre Les Nancy

The following supporting material discusses the construction of the Pourbaix diagram of lanthanum. This diagram, which is presented in Fig. S1, provides an alternative view of the conditions for which solution certain lanthanum species are predominant.

In aqueous media, lanthanide elements are known to be subjected to chemical reactions in which proton transfer and/or electron transfer occurs. Therefore, the corresponding Pourbaix diagrams are composed of three types of lines:

1) Horizontal lines when species transitions only involve electron(s) transfer. The Nernst equation was used to calculate the reduction potential at which the concentrations of two species are equal:

$$\mathbf{E} = \boldsymbol{E^0}_{ox/red} + \frac{\mathbf{RT}}{\mathbf{nF}} \mathbf{ln}\left(\frac{a_{ox}}{a_{red}}\right) \leftrightarrow \mathbf{E}_{eq} = \boldsymbol{E^0}_{ox/red},$$

where E and E^0 are the electrochemical potential (V) and standard reduction potential (V), respectively, R is the perfect gas constant, T is the temperature in K, F is the Faraday constant (96485J/V.mol), a_{red} is the activity of the reductant, a_{ox} is the activity of the oxidant, n is the stoichiometric quantity of electrons transferred, and K is the reaction constant. The standard reduction potential E^0 was calculated from the following equation, where ΔG_r^0 is the Gibbs standard free energy of reaction:

$$E^0 = \frac{\Delta G_r^0}{-nF}$$

The Gibbs standard free energy of formation of La^{3+} species is presented in Table S1. The other Gibbs standard free energies of formation of the La (III) species used in this study were calculated from the reaction constants listed in Table S2 using the Gibbs standard free energies of formation of La^{3+} and the van't Hoff equation: $\Delta G_r^0 = -RTln(K)$.

2) Vertical lines when reactions only involve proton(s) transfer. These reactions can be written as follows:

$$La(OH)_i^{3-i} + h \times H^+ = La(OH)_{i+h}^{3-i-h} + h \times H_2O$$

The pH at which the concentrations of two species are equal may be calculated by using the following equation and reaction constants listed in Table S2:

$$pH_{equilibrium} = \log(K) \times \frac{1}{h},$$

where *h* is the stoichiometric quantity of protons transferred.

3) Diagonal lines when both electron and proton transfer are involved. A developed form of the Nernst equation was used to calculate the conditions (reduction potential and pH) under which the concentrations of two species are equal:

$$E = E^0 - \frac{hRTln(10)}{nF}\text{pH} + \frac{RTln(10)}{nF}\log\left({[A]}/{[B]}\right) \quad \leftrightarrow \quad E_{eq} = E^0 - \frac{0.0591h}{n}\text{pH}_{eq}$$

In the same manner as that for horizontal lines, the Gibbs standard free energies of formation listed in Table S1 or back-calculated from the reaction constants listed in Table S2 were used to calculate the standard reduction potential E^0.

Table S1: Gibbs standard free energies of formation used to construct the Pourbaix diagrams

Species	$\Delta G^{o}_{f,298}$ (kJ mol^{-1})	Reference
H_2O	−237.1	(Lide, 2005)
OH^-	−157.2	(Lide, 2005)
La^{3+}	−697.1	(Outotec, 2018)

Table S2: Back-calculated hydroxylation reaction constants used to construct the Pourbaix diagrams

Reaction	Reaction constant	Reference
$La^{3+} + H_2O = La(OH)^{2+} + H^+$	$\beta_{1,1}^{*}=10^{-8.6}$	(Kragten et al., 1987)
$La(OH)^{2+} + H_2O = La(OH)_2^{+} + H^+$	$\beta_{2,1}^{*} / \beta_{1,1}^{*}=10^{-9.3}$	(Kragten et al., 1987)
$La(OH)_2^{+} + H_2O = La(OH)_3 + H^+$	$\beta_{3,1}^{*} / \beta_{2,1}^{*}=10^{-9.4}$	(Kragten et al., 1987)

* Back-calculated

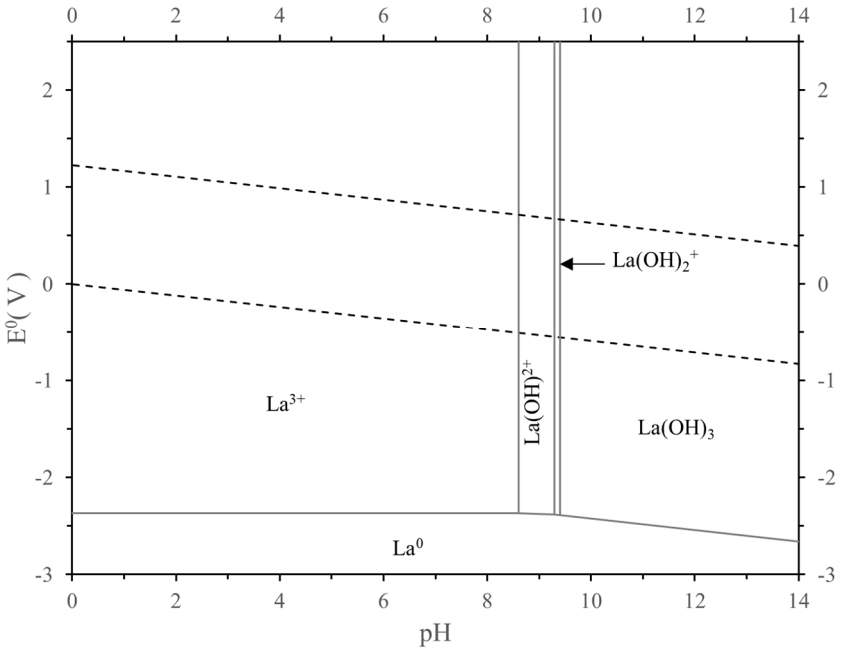

Fig. S1: Pourbaix diagram of lanthanum in aqueous media

D.R. Lide, CRC Handbook of Chemistry and Physics, 85th ed., CRC Press, Boca Raton, Florida, USA, 2005.
Outotec, HSC Chemistry 9, (2018).
J. Kragten, L.G. Decnop-Weever, Hydroxide complexes of lanthanides-VIII: Lanthanum(III) in perchlorate medium, Talanta. 34 (1987) 861–864. doi:10.1016/0039-9140(87)80115-7.